Inorganic Chemistry

Article

pubs.acs.org/IC

Correlations between Chemical Bonding and Magnetic Exchange Interactions: Synthesis, Crystal Structures, and Magnetic Properties of the New Family RE_2AlGe_2 (RE = Tb−Tm, Lu)

Jiliang Zhang and Svilen Bobev*

Department of Chemistry and Biochemistry, University of Delaware, Newark, Delaware 19716, United States

Supporting Information

ABSTRACT: Six new rare-earth metal germanides with general formula $RE_2Al_{1-x}Ge_{2+x}$ (RE = Tb−Tm, Lu; $0.13(2) \leq x \leq 0.37(2)$) have been synthesized by direct fusion of the corresponding elements. Their structures have been established by single-crystal diffraction to crystallize with the orthorhombic space group *Immm* (no. 74), adopting the W_2CoB_2 structure type. The Al and Ge atoms are arranged in alternating planar layers, made of rhombic- and hexagonal-fragments. The rare-earth metal substructure consists of puckered four-connected nets. Electronic structure calculations support the coloring of the Ge and Al sites and account for the existence of a small homogeneity range. DC magnetization measurements for all specimens are also presented; based on the RKKY and mean-field theories for antiferromagnets, relationships between the chemical bonding and exchange interactions are discussed.

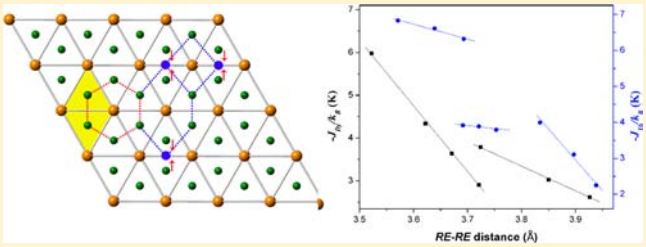

INTRODUCTION

Prior investigations in the rare-earth (RE) metal−germanium systems near the $REGe_2$ compositions have revealed intricate structural chemistry.[1−6] A characteristic feature here is the occurrence of a variety of nonstoichiometric $REGe_{2-x}$ phases with the AlB_2- and α-$ThSi_2$-structure types (light rare-earths) or $REGe_2$ phases adopting the $ZrSi_2$-type (heavy rare-earths).[1] Recent work has also shown that there are multiple superstructures based on these three structure types.[2] The interesting structural chemistry and the rich magnetic properties make such materials worthy candidates for the investigation of the structural evolution and structure−properties relationships in rare-earth metal compounds.

While it is generally agreed that a combination of geometric and electronic factors governs the structure formation, a complete understanding of why and how specific interactions arise in binary or ternary systems is still lacking. A useful way to understand the mechanism for structural variations is the doping (or "alloying") of a third element with different size and/or number of valence electrons. It is also clear that varying the content of the third element can lead to (dis)continuous structural evolution,[1a] which can be suitably followed within the realm of the "coloring" problem.[3]

Our earlier work on rare-earth metal germanides "alloyed" with various elements from neighboring groups nicely demonstrates the above points: extended families of RE_2XGe_2 (X = Mg, In, Cd; U_3Si_2-type) compounds[4] can be formed and their magnetic properties studied. These results suggest that this particular arrangement is not strongly influenced by the atomic size and/or the electronic configuration of the "foreign" element, yet attempts to synthesize the isotypic RE_2GaGe_2 have been unsuccessful so far. After the failure to extend this chemistry toward Ga, we reasoned that this structure (most likely) will not be realized with Al either but nonetheless decided to explore these systems; after all, Dy_2AlGe_2 was already reported before this work commenced.[5] With this paper, we present a brief summary of our exploratory work and report the structures of six new compounds formed with the heavy rare-earths metals Tb−Tm and Lu. These RE_2AlGe_2 phases (rather $RE_2Al_{1-x}Ge_{2+x}$; $0.13(2) \leq x \leq 0.37(2)$) crystallize with the orthorhombic W_2CoB_2 type and exhibit small homogeneity ranges. For the sake of simplicity, hereafter, they are referred to as RE_2AlGe_2. Discussed as well are the specifics of the magnetic response of these materials, such as ordering temperatures, empirical relationships between RE−RE separations, and exchange interactions.

EXPERIMENTAL SECTION

Synthesis. All initial manipulations were performed inside an argon-filled glovebox with controlled oxygen and moisture levels below 1 ppm or under vacuum. The starting materials—rare-earth metals (pieces, purity >99.9 wt.% metal basis, Ames Lab or Hefa) and Al (shot, purity 99.999 wt.%, Alfa-Aesar) were used as received. Ge (lump, purity 99.999 wt.%, Acros) was melted into an ingot using an arc-melter before use. All samples (nominal composition RE:Al:Ge = 2:1:2) were prepared by arc-melting the elemental constituents under Ti-gettered Ar gas atmosphere. Each button was remelted and flipped at least three times to ensure homogeneity. Weight losses were minimal (<0.5 wt.%), and the obtained materials were sealed into evacuated fused silica ampules for further heat-treatment. This was

Received: January 31, 2013
Published: April 23, 2013

   dx.doi.org/10.1021/ic400254v | *Inorg. Chem.* 2013, 52, 5307−5315

Table 1. Selected Crystallographic Data for $RE_2Al_{1-x}Ge_{2+x}$ (RE = Tb−Tm, Lu; 0.13(2) ≤ x ≤ 0.37(2))

	empirical formula					
	$Tb_2Al_{0.87}Ge_{2.13(2)}$	$Dy_2Al_{0.80}Ge_{2.20(2)}$	$Ho_2Al_{0.77}Ge_{2.23(2)}$	$Er_2Al_{0.67}Ge_{2.33(2)}$	$Tm_2Al_{0.63}Ge_{2.37(2)}$	$Lu_2Al_{0.79}Ge_{2.21(1)}$
formula weight	495.53	506.28	512.51	521.73	526.90	531.91
temperature	200(2) K					
radiation	Mo Kα, λ = 0.71073 Å					
space group	*Immm*, Z = 2					
a (Å)	4.0998(11)	4.0698(5)	4.0572(12)	4.0349(6)	4.0148(8)	4.0142(14)
b (Å)	6.0034(16)	5.9827(7)	6.0113(17)	6.0513(10)	6.0467(11)	6.011(2)
c (Å)	8.692(2)	8.6051(10)	8.538(2)	8.4456(13)	8.3818(16)	8.349(3)
V (Å^3)	213.92(10)	209.52(4)	208.23(10)	206.21(6)	203.48(7)	201.48(12)
ρ_{cal} (g cm^{-3})	7.699	8.025	8.174	8.403	8.600	8.768
μ (cm^{-1})	474.17	508.01	534.35	569.79	603.84	648.46
final residuals ($I > 2\sigma_I$)[a]	R_1 = 0.0174	R_1 = 0.0189	R_1 = 0.0141	R_1 = 0.0146	R_1 = 0.0213	R_1 = 0.0136
	wR_2 = 0.0396	wR_2 = 0.0439	wR_2 = 0.0371	wR_2 = 0.0330	wR_2 = 0.0524	wR_2 = 0.0305
final residuals (all data)[a]	R_1 = 0.0199	R_1 = 0.0193	R_1 = 0.0147	R_1 = 0.0155	R_1 = 0.0228	R_1 = 0.0146
	wR_2 = 0.0412	wR_2 = 0.0439	wR_2 = 0.0373	wR_2 = 0.0331	wR_2 = 0.0530	wR_2 = 0.0307
largest difference peak/hole (e$^-$ Å^{-3})	1.90/−1.26	1.83/−1.69	1.33/−1.47	1.29/−1.41	1.66/−2.23	1.52/−1.05

[a] $R_1 = \sum||F_o| - |F_c||/\sum|F_o|$, $wR_2 = \{\sum[w(F_o^2 - F_c^2)^2]/\sum[w(F_o^2)^2]\}^{1/2}$, where $w = 1/[\sigma^2F_o^2 + (AP)^2 + BP]$, and $P = (F_o^2 + 2F_c^2)/3$; A and B are weight coefficients; see CIF in Supporting Information.

deemed necessary because secondary phases were present in the as-cast specimens, $REGe_{2-x}$ most frequently. To obtain single-phase products, annealing at different temperatures was carried out in conjunction with TG/DTA experiments; on the basis of the above and the corresponding powder X-ray diffraction patterns, it can be suggested that the best route toward high-purity RE_2AlGe_2 samples is annealing at 1273 K for longer than 2 weeks. Annealing at a higher temperature appears to increase the amount of $REGe_{2-x}$ (the peaks in the powder X-ray diffraction patterns originating from the AlB_2-type subcell increased in intensity compared between as-cast and annealed samples), while lower temperature showed no difference (likely because much longer annealing time is needed).

As shown in Table 1, the refined formula in all cases deviates from the ideal 2:1:2 stoichiometry, which may imply the existence of small impurities, even in samples that appear to be phase-pure based on their powder X-ray diffraction patterns. We did try to assess the compositional range, which can be also seen from the slight shift of the peaks' positions in the powder diffraction patterns, but those attempts only proved that the material is always substoichiometric with regard to aluminum and the phase width is very small. All efforts to obtain the compositions RE_2AlGe_2 or $RE_2Al_{1+x}Ge_{2-x}$ failed.

Yb_2AlGe_2 could not be made despite repeated attempts. The arc-melting route was not deemed suitable for Yb due to its relatively low vapor pressure and substantial weight-loss during the process. To make Yb_2AlGe_2 samples, the constituting elements were sealed into Nb tubes and melted by an induction heater. Then the Nb tubes were enclosed into the evacuated silica tubes, which were quickly (rate 200 K/h) heated to 1373 K and kept for 2 days, followed by slow cooling (rate 2 K/h) to 1273 K. The major product was $Yb_{11}Ge_{10}$.

Extending the RE_2AlGe_2 series toward the light rare-earth metals was also not possible within the scope of this work. For example, all Gd-containing melts always yielded $Gd(Al,Ge)_2$ (α-$GdSi_2$-type structure) as nearly single phase for a wide range of Al/Ge ratios. Gd_2AlGe_2 is known from the work of Choe et al., but it adopts a different structure (a monoclinic stacking variant of the W_2CoB_2).[6]

X-ray Powder Diffraction. X-ray powder diffraction patterns were taken at room temperature on a Rigaku MiniFlex powder diffractometer using filtered Cu Kα radiation. The obtained patterns were then compared with the calculated patterns based on the corresponding single-crystal structures, and they matched very well to one another. Representative X-ray powder diffraction patterns are provided in Figure S1 (Supporting Information). Polycrystalline RE_2AlGe_2 samples appear stable in air for periods greater than 3 months.

Single Crystal X-ray Diffraction. Crystals were selected from the reaction products and were cut under a microscope to ca. 0.07−0.08 mm in all dimensions. They were placed on glass fibers using Paratone N oil. Intensity data sets were collected at 200 K on a Bruker SMART CCD-diffractometer equipped with monochromated Mo Kα radiation. SMART[7] and SAINTplus[8] programs were employed for the data collection and integration of the frames, respectively. SADABS was used for semiempirical absorption correction based on equivalents.[9] The structures were solved by direct methods and refined on F^2 with the aid of the SHELXTL package.[10] A list of important crystallographic parameters and details for these refinements are summarized in Table 1. Final positional and isotropic thermal parameters and important distances for the Dy compound are listed in Tables 2 and 3,

Table 2. Atomic Coordinates and Equivalent Isotropic Displacement Parameters (U_{eq}[a]) of Dy_2AlGe_2

atom	site	x	y	z	U_{eq} (Å^2)
Dy	4*f*	0	1/2	0.7861(1)	0.006(1)
Al[b]	2*a*	0	0	0	0.010(1)
Ge	4*h*	0	0.2131(1)	1/2	0.010(1)

[a] U_{eq} is defined as one-third of the trace of the orthogonalized U^{ij} tensor. [b] Refined as Al:Ge = 0.80:0.20(2).

Table 3. Selected Interatomic Distances in Dy_2AlGe_2

atom pair	distance (Å)	atom pair	distance (Å)
Dy−Al (× 2)	3.1942(5)	Al−Ge (× 4)	2.6620(9)
Dy−Ge (× 2)	3.0013(9)	Ge−Ge	2.550(3)
Dy−Ge (× 4)	3.0255(7)	Dy−Dy (× 2)	3.6709(4)

respectively. The corresponding data for the remaining isotypic compounds are given in the Supporting Information (Tables S1 and S2). The combined crystallographic information file (CIF) is provided as Supporting Information as well.[11]

Elemental Microanalysis. Crystals from each sample were picked and mounted onto carbon tape. The analysis was performed using a JEOL 7400 F electron microscope equipped with an INCA-Oxford energy-dispersive spectrometer. The microscope was operated at 10 μA beam current at 15 kV accelerating potential. Data were acquired for several spots on the same crystal and averaged. The obtained elemental ratios are in good agreement with the refined compositions (Figure S2 in Supporting Information).

dx.doi.org/10.1021/ic400254v | Inorg. Chem. 2013, 52, 5307−5315

Magnetic Properties. Field-cooled DC magnetization measurements were conducted using a Quantum Design PPMS system from 300 to 5 K under applied fields of 500 Oe. For the Lu compound, magnetization from 300 to 2 K was measured under an applied field of 100 Oe (the lower field was used to discern a possible superconducting transition). The raw magnetization data were corrected for the holder contribution and converted to molar susceptibility (χ_m = M/H).

Electronic Structure Calculations. Tight-binding linear muffin-tin orbital (TB-LMTO) calculations were performed on a fully ordered and optimized Lu_2AlGe_2 structure in the atomic sphere approximation (ASA).[12] The radii of the Wigner−Seitz (WS) spheres were assigned automatically so that the overlapping potential would be the best possible approximation to the full potential.[13] They were determined as follows: Lu = 1.804 Å, Al = 1.469 Å, and Ge = 1.404 Å. The *k*-space integrations were conducted by the tetrahedron method,[14] and the self-consistent charge density was obtained using 12 × 12 × 12 *k*-points in the Brillouin zone. Lu 6p, Al 3p, and Ge 4d orbitals were downfolded while the Lu 4f[14] were treated as core.[15] Exchange and correlation were treated by the local density approximation,[16] and all relativistic effects were taken into account using scalar relativistic approximation,[17] except spin−orbit coupling. To interrogate the chemical bonding, crystal orbital Hamilton populations (COHP)[15] of selected interactions were also analyzed.

Total energy calculations for structural optimization of the idealized Lu_2AlGe_2 compound were performed with the first-principle pseudopotential-based density functional theory as implemented in SIESTA,[18,19] which employs a localized orbital basis in the representation of wave functions. We used soft norm-conserving pseudopotential and the Perdew−Berke−Emzerhof exchange correlation energy within the generalized gradient approximation.[20,21] The optimizations are deemed to have sufficiently converged when the residual forces on any atoms are smaller than 0.001 eV/Å.

RESULTS AND DISCUSSION

Synthesis, Structure, and Bonding. RE_2AlGe_2 (RE = Tb−Tm, Lu) are the first germanides with the orthorhombic W_2CoB_2-structure type (Pearson symbol *oI*10). The isostructural RE_2AlSi_2 (RE = Ho−Tm, Lu) silicides,[22] however, are already known. As mentioned already, Gd_2AlGe_2 does exist[6] but adopts a monoclinic stacking variant of this structure; stoichiometric Dy_2AlGe_2 is also known, but it crystallizes with the Mo_2FeB_2-type structure.[5] All of the above is suggesting that the same bonding arrangement cannot be extended beyond the late lanthanides. Furthermore, it seems that small phase width in $RE_2Al_{1-x}Ge_{2+x}$ ($0.13(2) \le x \le 0.37(2)$), which is due to the partial substitution of Al with Ge at the Al site, is an inherent feature of the structure[23] because it raises the valence electron concentration (VEC); the slightly higher VEC appears to be favored for the anionic network in question, while the VEC for the stoichiometric RE_2AlGe_2 (RE = Gd, Dy) compounds is likely favored for different polyanionic arrangements.[5,6] Further details on this aspect of the bonding are discussed in the electronic band-structure section.

The structure is schematically presented in Figure 1. It is rather simple, with three unique atoms in the asymmetric unit (Table 2). It can be described as two-dimensional (2D) flat sheets of Al and Ge atoms (polyanionic substructure), and puckered layers of RE-metal atoms (cationic substructure) between them.

There is a shift between neighboring Ge/Al layers halfway along the *c*-axis. The layers themselves can be broken to $[Ge_2Al_2]$ "squares" and $[Ge_4Al_2]$ "hexagonal rings" as demonstrated in Figure 2. The "square" unit is commonly seen in binary RE-germanides with the α-$ThSi_2$- and $ZrSi_2$-type structures (and their derivatives), as well as in the REAlGe

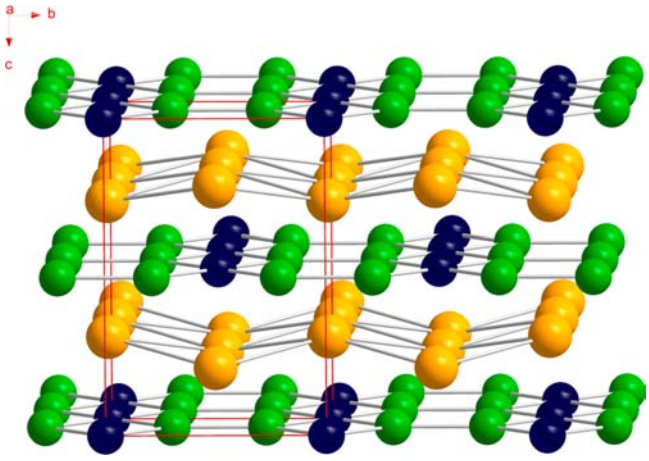

Figure 1. Schematic representation of RE_2AlGe_2, viewed approximately along the crystallographic *a*-axis. RE atoms are represented as gold spheres, Ge atoms are drawn as green atoms, and Al atoms (actually statistically disordered Al and Ge) are shown with blue spheres. The unit cell is outlined by the red frame.

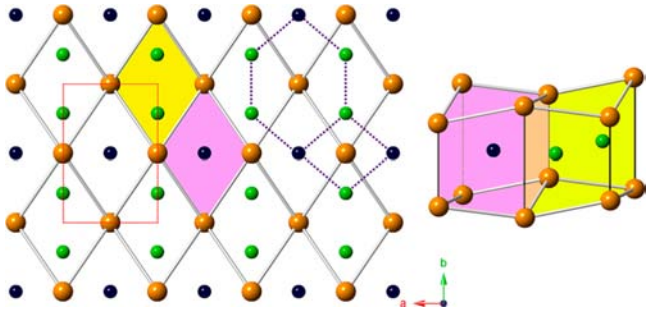

Figure 2. Projection of the crystal structure of RE_2AlGe_2 on the (001) plane. The red dotted line shows the unit cell, and the blue dotted line emphasizes the "square" and "hexagonal" fragments making up the polyanionic Al/Ge sheets. The RE_8-polyhedra around the Ge_2-dumbbells and the Al atoms are rendered in yellow and pink, respectively. The deformation of the trigonal prims is represented in the panel to the right. Rare-earth metal atoms are represented as gold spheres, Ge atoms are drawn as green spheres, and Al atoms are shown in blue.

compounds with the YAlGe-type.[24] The "hexagonal rings" are a hallmark in the crystal chemistry of binary RE-germanides with the AlB_2-type structure and its derivatives, as well as the $Eu_3Al_2Ge_2$ structure.[25]

The structure can also be characterized as the intergrowth of $[RE_8]$ blocks, which are essentially two trigonal prisms or rare-earth metal atoms sharing a common rectangular face. Each of these units is centered by Al atoms and Ge−Ge dimers, respectively. Such uneven occupation of the $[RE_6]$ trigonal prisms, which are very common structural motifs in the crystal chemistry of many RE-germanides, leads to the observed deformation of the $[RE_8]$ "cube", as shown in Figure 2. Considerably less distorted RE_8-polyhedra with cubic/rectangular-prismatic shape are also known in the RE_2XGe_2 (X = Mg, In, Cd; U_3Si_2-type, i.e., Mo_2FeB_2-type structure),[4] where the heteroatoms are located. Note that in the latter structure, $[RE_6]$ trigonal prisms host the Ge atoms as well; thereby, both the Mo_2FeB_2-type and W_2CoB_2-type structures should be considered as close relatives to the AlB_2-type structure. The differences between the "2−1−2" structures are very subtle, indeed, and most likely the smaller size atom in the $[RE_8]$

dx.doi.org/10.1021/ic400254v | Inorg. Chem. 2013, 52, 5307−5315

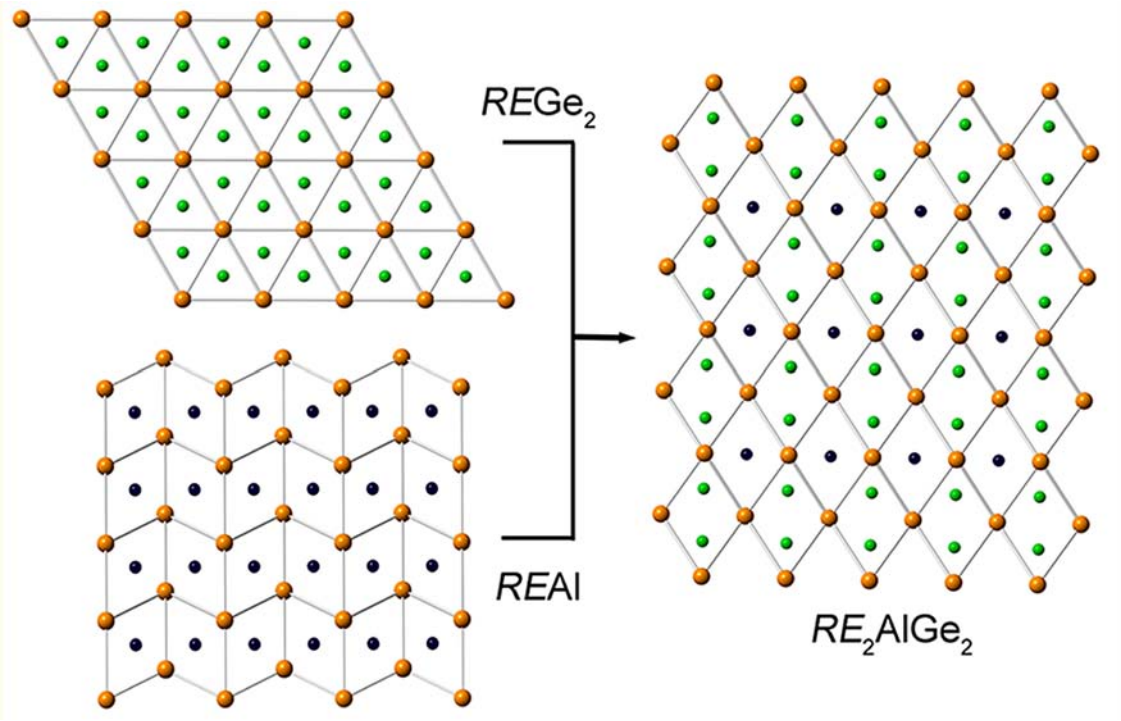

Figure 3. Schematic representation of the structural relationship between the RE_2AlGe_2 and the structures of $REGe_2$ (AlB_2-type structure) and REAl (CsCl-type structure, distorted from the actual cubic symmetry to guide the eye). The structure of title compound can be regarded as their 1:1 intergrowth. RE atoms are represented as gold spheres, Ge atoms are drawn as green spheres, and Al atoms are shown in blue.

"cube" in RE_2AlGe_2 (r_{Al} = 1.248 Å)[26] compared to RE_2InGe_2 (r_{In} = 1.421 Å)[26] causes the distortions. In this view, the RE_2AlGe_2 structure can be thought to be an intergrowth of the imaginary $REGe_2$ and REAl fragments with a 1:1 ratio, as shown in Figure 3. The same approach can be used to rationalize the structures of the RE_2XGe_2 (X = Mg, In, Cd; U_3Si_2-type) compounds,[4] as well.

The Ge−Ge distances in RE_2AlGe_2 vary between 2.534(3) Å and 2.571(2) Å, subject to the varied Al:Ge ratio and the nature of the rare-earth metal (Table 3 and Table S2). The average of the Ge−Ge distances (ca. 2.55 Å) is longer than the Ge−Ge distance in elemental Ge[26] but comparable to the Ge−Ge distances in RE_2XGe_2 (X = Mg, In, Cd).[4] The Al atoms are in atypical planar four-coordinate environment with Al−Ge distances in the range of 2.6620(9) Å to 2.6733(8) Å. Similar distances are known for structurally related compounds such as Gd_2AlGe_2,[6] RE_2AlGe_3,[27] $RE_2Al_3Ge_4$,[28] $Eu_3Al_2Ge_2$,[25] and $Yb_7Al_5Ge_8$,[29] among others.

With regard to the interatomic distances, we also point out a peculiarity in the unit cell volumes (Table 1); nominally, one would expect them to follow the lanthanide contraction, which they do. However, the changes in the Al content seem to have a very large "anisotropic" effect; the lattice constant *b* shows a local maximum around Er_2AlGe_2 and Tm_2AlGe_2, where the Al content is minimized. With aluminum being slightly larger than germanium (r_{Al} = 1.248 Å, r_{Ge} = 1.242 Å),[26] it is counter-intuitive that such elongation happens. This observation is also supported by the structure optimizations by SIESTA,[18,19] which show that the optimized structure of the stoichiometric compound Lu_2AlGe_2 has a larger unit cell volume compared to $Lu_2Al_{0.79}Ge_{2.21(1)}$, which is in line with the increased Al concentration; nonetheless, the *b*-axis is shortened in the calculations (vide infra). It is therefore logical to expect that the Al−Ge disorder will not only have a "geometric" effect but will also subtly influence the chemical bonding as well. Careful examination of the anisotropic displacement parameter of the Al site reveals $U_{22} \approx 3 \times U_{11}$, which is more pronounced in the structures with lowest Al concentration (Table S3 in Supporting Information). Although it is not possible to split this site and model the disorder in a better way, on the basis of the above, we may speculate that if higher substitution rate of Ge for Al was possible, the structure could rearrange to adapt the AlB_2-type structure. Such hypothetic transformation can be derived by splitting of Al site in the *b* direction and replacing the Al atom with a Ge_2 dumbbells, as schematically illustrated in Figure 4. The high-temperature transformation to AlB_2-related structure supports this line of thinking as well.

Electronic Structure. Computations based on the density functional theory were carried out for Lu_2AlGe_2 compound with optimized structure by SIESTA.[18,19] The optimized lattice parameters are *a* = 4.0267 Å, *b* = 5.9863 Å, and *c* = 8.4257 Å. The total and partial density of states (DOS) curves and the COHPs calculated for the Al−Ge and Ge−Ge bonds in Lu_2AlGe_2 are plotted in Figure 5.

As evident from the total DOS in Figure 5, the Fermi level of the optimized structure is located at a small peak, corresponding to a relatively high DOS, while a deep valley (or pseudogap) appears at just 0.45 eV above the Fermi level. The flat bottom of the DOS valley suggests that the structure stands in a range of VEC, in good agreement with the experimental results. Such characteristics of the total DOS indicate that the stoichiometric compound Lu_2AlGe_2 is not favored electronically, and a slightly higher VEC is required to stabilize the structure. The shift of the Fermi level from the present peak shoulder (for the Lu_2AlGe_2 compound) to the pseudogap (for the $Lu_2Al_{1-x}Ge_{2+x}$ compound) by virtue of increasing the number of valence electrons not only stabilizes the electronic structure but also diminishes its metallicity.

dx.doi.org/10.1021/ic400254v | Inorg. Chem. 2013, 52, 5307−5315

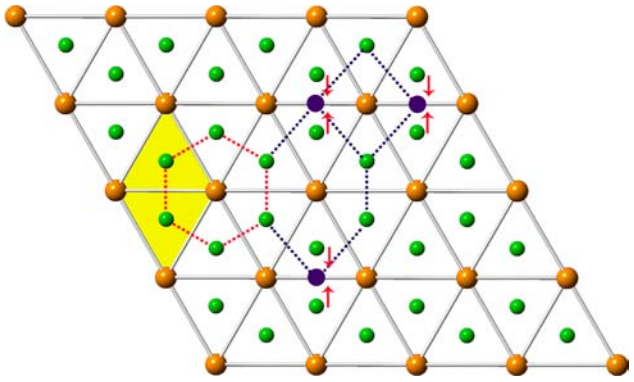

Figure 4. Schematic illustration of structural "evolution" of the $RE_2Al_{1-x}Ge_{2+x}$ ($0.13(2) \leq x \leq 0.37(2)$) structure toward the AlB_2-type structure. The $[Al_{1-x}Ge_{2+x}]$ polyanionic layers try to adapt to the changes in the VEC as more Ge replaces Al, causing small positional disorder at the Al site. The red dotted lines outline the hexagonal ring in the AlB_2 structure, and the blue dotted lines depict the structure under consideration. RE atoms are represented as gold spheres, Ge atoms are drawn as green spheres, and Al atoms are shown in blue.

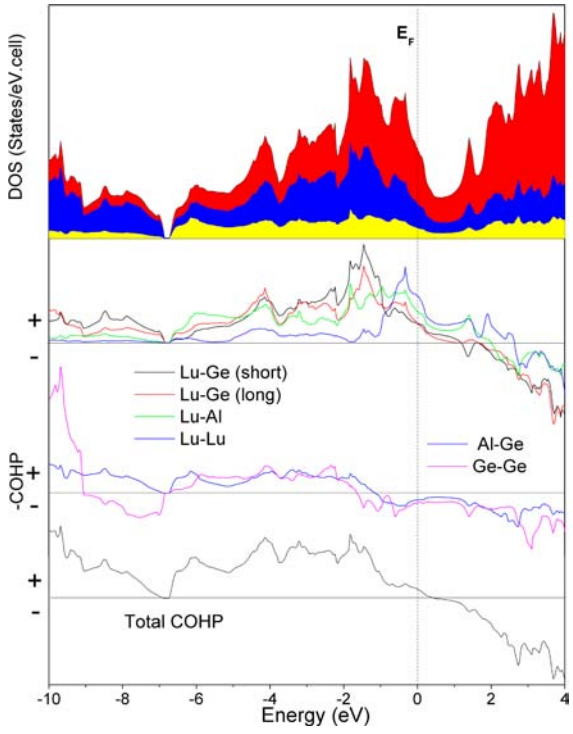

Figure 5. Calculated DOS and COHP for an idealized Lu_2AlGe_2 structure. The partial DOS curve for Ge is shown by the blue area; Al and Lu partial DOS are shown by the yellow and red areas, respectively. The COHP curves refer to individual interactions. The Fermi level is chosen as the energy reference at 0 eV.

According to the COHPs for the optimized structure (Figure 5), both Al–Ge and Ge–Ge bonds show weakly antibonding character at the Fermi level, and a slightly higher VEC (partial substitution of Al by Ge) is not expected to have a significant effect on the bonding within the polyanionic substructure. Although these interactions are represented by similar distances to those in other AlB_2-type structures, the bonding should be weakened due to the increased antibonding character. In contrast, a strengthening of the RE–RE bonding can be clearly seen from their shorter separations in (Tables 3 and S2) and should have a more significant contribution here.

Magnetic Susceptibilities. The magnetization data of the RE_2AlGe_2 (RE = Tb–Tm) samples are plotted in Figure 6. From the plots of the magnetic susceptibility (χ = M/H) as a function of temperature (T), it is clearly seen that all samples are paramagnetic and obey the Curie–Weiss law[30] in the high-temperature regime. The paramagnetic Curie temperature θ_p and effective moment p_{eff} of the compounds can be obtained from the linear regression of the inverse magnetic susceptibility against temperature as demonstrated in inset in Figure 6, and the numerical parameters are summarized in Table 4.

These observed moments were consistent with the values expected for free ion RE^{3+} species according to Hund's rule.[30] The positive Curie temperature in the Tb compound likely suggests the existence of strong ferromagnetic interactions, as in the case of $EuAl_4$.[31] In the low-temperature region, typical antiferromagnetic behavior can be inferred from the cusp of the magnetization data and the relatively low magnetic susceptibilities. Two transitions are observed for $Tb_2Al_{1-x}Ge_{2+x}$, while all other samples show only one;[32] the corresponding ordering temperatures are summarized in Table 4. The dependence of the Néel temperature (T_N) on the de Gennes factors[33] ($G=J(J+1)(g-1)^2$, where J is the total angular momentum and g is the Landé constant) is given in Figure 7.

The ordering temperatures of Tb, Dy, and Er compounds follow a good linearity, confirming the expected RKKY interactions.[34] The Néel temperature of the Ho compound deviates from the linear fit. Compared with other rare-earth metal germanides, the title Tb- and Dy-compounds show much higher ordering temperature and only the REGe compounds have close ordering temperatures.[35] To gain more insight into the possible structural origin of such high ordering temperature here, an evaluation of the ordering temperatures on various other RE-based germanides (≥50 at.% Ge) was performed and is graphically represented in Figure 8.

These germanides include REGe,[35] RE_3Ge_4,[36] RE_3Ge_5,[2a,37] RE_2MgGe_2,[4c] and selected $REGe_{2-x}$ of different structure types.[38,39] It is obvious that for Tb-based germanides, the ordering temperature varies most significantly, largely dependent on the structure; the range narrows notably for the compounds of the heaviest rare-earths. Specifically, the ordering temperature of the Tm-based germanides is always ca. 2 K. The value is also very close to the extrapolated ordering temperature of the TmBiGe compound.[40] If the value was also taken as the ordering temperature of Tm_2AlGe_2 here, another linear relationship is revealed as shown in Figure 7, indicating the role of another RE magnetic sublattice (different s–f exchange coupling), according to the Néel's two-lattice theory.[41] We can also point that prior investigations on numerous intermetallic compounds have revealed that Gd-, Tb-, and Dy-based phases are generally with colinear magnetic structures and small crystal anisotropy, while the Ho-, Er-, Tm-counterparts are with helical magnetic structures and large crystal anisotropy.[42] It is evident that such noncolinear structures and large crystal anisotropy will depress the role of the RE–RE separation in the mediation of the exchange interactions, as seen in Figure 8.

Within the context of this discussion, we were intrigued by the significant difference between the ordering temperatures of Tb_2AlGe_2 and Dy_2AlGe_2 (Table 4). After all, the introduction of a main-group element on the magnetic response of RE-based compounds should be accounted for by the RKKY theory.[34] Further, among the Dy-based germanides, DyGe and Dy_2AlGe_2

dx.doi.org/10.1021/ic400254v | Inorg. Chem. 2013, 52, 5307–5315

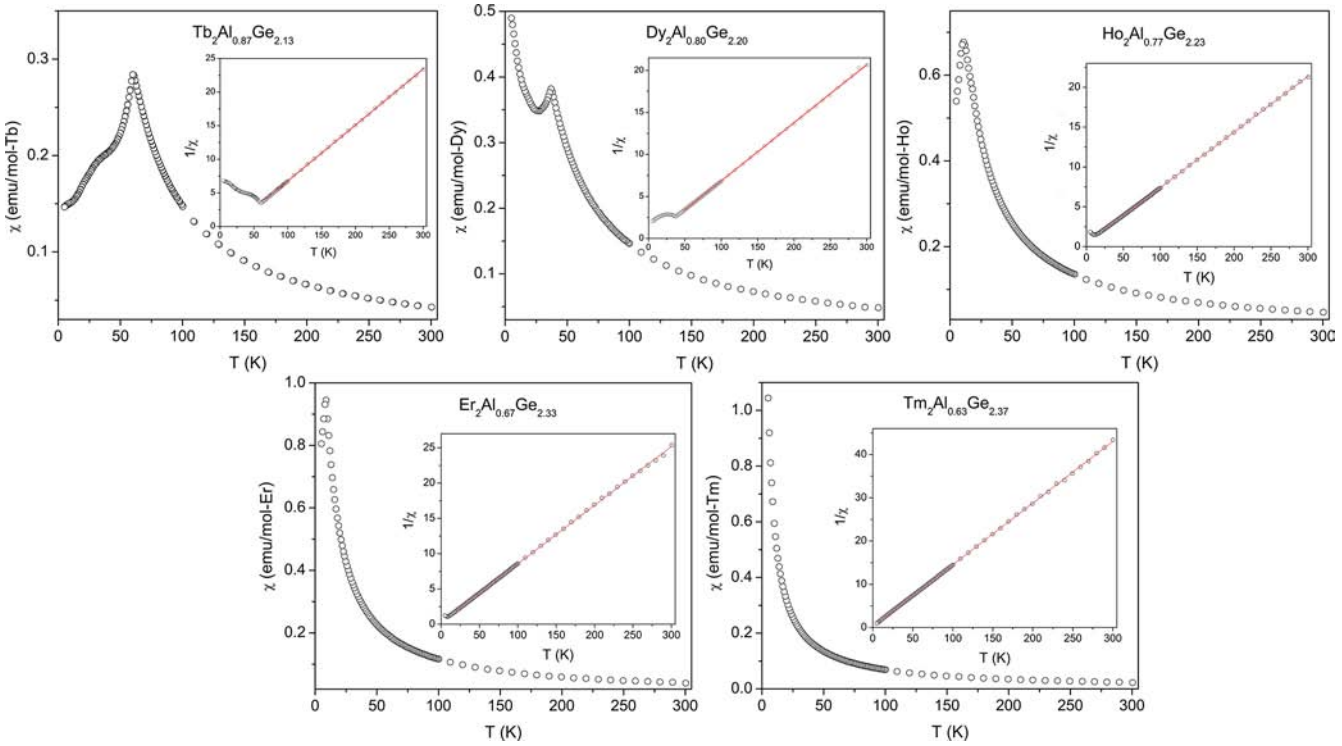

Figure 6. Temperature dependence of the magnetic susceptibility $\chi(T)$ for polycrystalline RE_2AlGe_2 (RE = Tb−Tm) samples. The insets show the inverse susceptibility $\chi^{-1}(T)$, and the red lines represent the linear fit to the Curie−Weiss law, attesting for the paramagnetic local-moment behavior in all five cases.

Table 4. Selected Magnetic Parameters for RE_2AlGe_2

compound	T_N (K)	θ_p (K)	p_{eff} (μ_B)	$g\sqrt{J(J+1)}$ (μ_B)
Tb_2AlGe_2	61, 32	16.4	9.86	9.72
Dy_2AlGe_2	37	1.0	10.76	10.63
Ho_2AlGe_2	12	−5.4	10.68	10.6
Er_2AlGe_2	8	−8.6	9.94	9.58
Tm_2AlGe_2	<5	−1.5	7.51	7.56

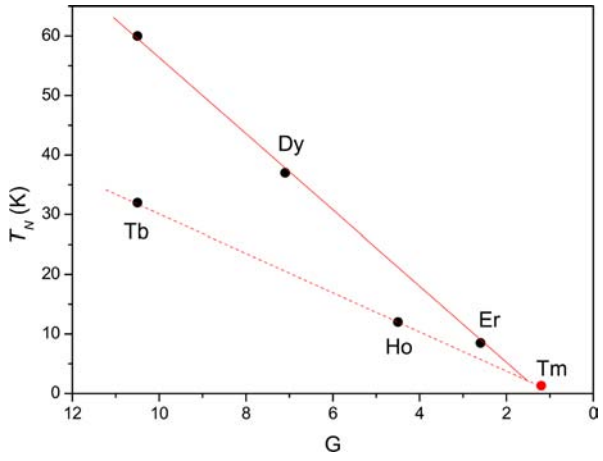

Figure 7. Néel temperatures of the RE_2AlGe_2 compounds, plotted as a function of the corresponding de Gennes factors.

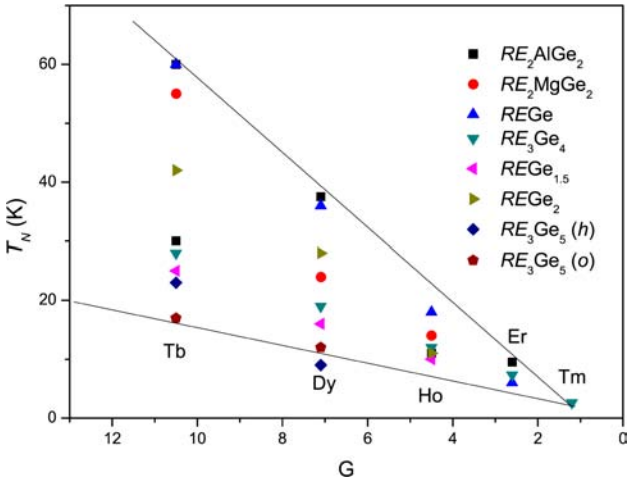

Figure 8. Néel temperatures in known RE−Ge binary and ternary compounds, plotted as a function of the corresponding rare-earth metal de Gennes factors. *h* denotes the hexagonal polymorphs, while *o* represents the orthorhombic one, where applicable.

are noted to have the highest ordering temperatures, which could be attributed to the relatively high RE-content. However, Dy_3Ge_4 which boasts slightly more than 42 at. % Dy (compared to 40 at. % in Dy_2AlGe_2), has much lower ordering temperature (Figure 8). Thus, this reasoning cannot account for the magnetic behavior alone. Because the topology of the magnetic sublattices in each case does not differ significantly (almost all are based on trigonal prismatic units), the other structural parameter that could influence the magnetic exchange is the interatomic distance. Indeed, the correlation between distance and ordering temperature has been already documented for many lanthanide and actinide compounds.[43,44] The correlation between distance and magnetic exchange interactions in transition metal-based amorphous alloys is also known within the formalism of the Bethe−Slater curve.[45] We "extrapolated" this knowledge and compared the shortest Dy−Dy separations

dx.doi.org/10.1021/ic400254v | Inorg. Chem. 2013, 52, 5307−5315

of all listed compounds and plotted the data vs the ordering temperatures; this regression confirmed that the shorter the separation, the higher the ordering temperature. Notable exception again is Dy_3Ge_4.

Generally, the local 4f moments of the RE atoms (in compounds with nonmagnetic elements) interact via RKKY-type interactions.[46] The RKKY model includes not only the RE−RE distances and the number of magnetic nearest neighbors but also the contribution from the conduction electrons, generally characterized by Fermi wave factor k_F. Thus, the ordering temperature of such RE-based antiferromagnets can be expressed as:[46]

$$k_B T_N = \frac{2}{3} J_T G \tag{1}$$

where J_T is the exchange interaction following

$$J_T = -12\pi n J_0 \sum_i F(2k_F R_i) \tag{2}$$

In the above equation, J_0 is a constant s−f exchange coupling integral, n is the average conduction electron to atom ratio, R_i is the distance between central magnetic atom and the ith magnetic atom, and $F(x)$ is an oscillating function. In the free electron model, the Fermi wave factor k_F can be evaluated as

$$k_F^3 = 3\pi^2 nN/V \tag{3}$$

where N is the total number of conduction electrons in a unit volume V.

Using eq 3, the k_F for the compounds listed in Figure 8 were calculated in a range of 1.625 $Å^{-1}$ ~ 1.722 $Å^{-1}$ for Dy and 1.619 $Å^{-1}$ ~ 1.717 $Å^{-1}$ for Tb, i.e., k_F varies very little. This could be due to the relatively high concentration of Ge in all compounds under consideration and the close valence electron concentrations for all. This has been noted before as the most likely the reason why the RE−RE separations and ordering temperatures could be well correlated (excluding the contribution of conduction electrons) in some lanthanide and actinide compounds.[43,44] Using this reasoning, we can also analyze the s−f exchange interactions in a simpler way.

According to the mean field theory, the exchange interaction mainly comes from the nearest exchange interaction. Thus the eq 2 can be simplified as

$$J_T = -12Z\pi n J_0 F(2k_F R) \tag{4}$$

where Z is the number of magnetic nearest neighbors. Using the determined Z value and the measured T_N, the s−f exchange interactions can be calculated using eq 1 and eq 4. The obtained values were then plotted against the shortest distance.[47] As shown in Figure 9a, the relationship between exchange interactions and distance (D) can be described by two linear fits: (i) J_0 = 25.8−6.4 × D, for D > 3.721 Å, and (ii) J_0 = 27.1−6.9 × D for D < 3.724 Å.[48] On the basis of these linear regressions, one can easily evaluate the s−f exchange integrals in RE germanides with >50% at. germanium. Using eqs 1 and 4, the calculated T_N are very close to the experimental results for the compounds in Figure 9a (the deviation is no more than 2 K). To further examine the validity of these empirical fittings, we calculated the ordering temperature of the $DyGe_3$ compound as 16.6 K: there are four nearest Dy neighbors in trigonal planar columns with distances of 3.90 Å and 3.92 Å.[49] The extrapolated value is very close to the experimental result of 16 K (Figure S4, Supporting Information). Also we can

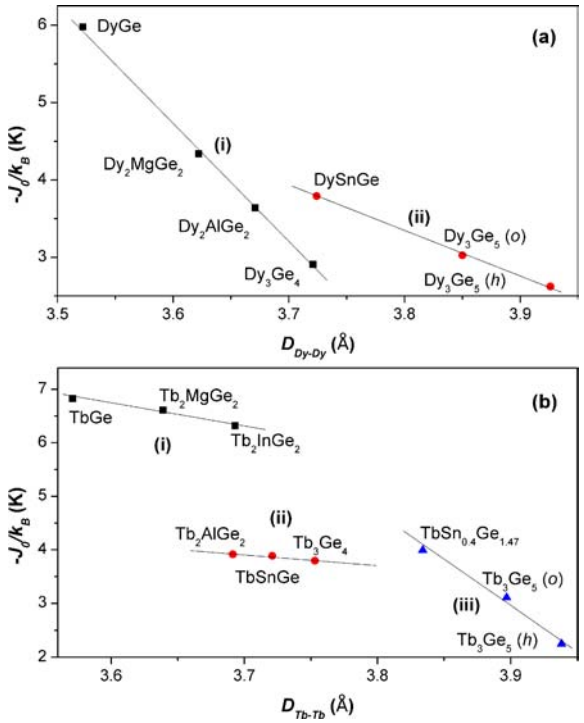

Figure 9. Magnetic exchange interactions vs the shortest RE−RE separation distance in germanides with (a) Dy and (b) Tb.

estimate the ordering temperature of Dy_2InGe_2 as 23.8 K, very close to that of Dy_2MgGe_2 (24 K).

The relationship between s−f exchange integrals and distances in the Tb-germanides can be characterized by three regions, as shown in Figure 9b: (i) $-J_0/k_B$ = 21.6−4.1 × D for D < 3.693 Å; (ii) $-J_0/k_B$ = 11.2−2.0 × D for 3.692 Å < D < 3.753 Å; (iii) $-J_0/k_B$ = 67.3−16.5 × D for D > 3.834 Å. The estimated deviation in ordering temperature is no more than 4 K from the fits. Evidently, the family following the de Gennes rule has similar s−f exchange energy, e.g., Dy_2AlGe_2 and Tb_2AlGe_2, DySnGe and TbSnGe. In contrast, the family without the de Gennes rule shows obvious difference in s−f exchange energy, e.g., Dy_3Ge_4 and Tb_3Ge_4, Dy_2MgGe_2 and Tb_2MgGe_2.

According to Figure 9b, the abnormally large slope in stage iii implies that the long Tb−Tb distance will dramatically reduce the s−f exchange coupling and thus the ordering temperature. It well accounts for the significantly different ordering temperature of Tb compounds in similar families. For instance, the $TbBi_{0.14}Ge_{1.74(2)}$ and $TbSn_{0.40}Ge_{1.47(1)}$ compounds show similar crystal structure and valence electron concentration but significantly different ordering temperatures: 13 K for the former and 26 K for the latter. According to Figure 9b, the nearest Tb−Tb separation for $TbBi_{0.14}Ge_{1.74(2)}$ is 3.908 Å, yielding a s−f exchange energy of 2.818 K. In the $TbSn_{0.40}Ge_{1.47(1)}$, the Tb−Tb separation is shorter, ca. 3.834 Å, yielding the s−f exchange energy of 4.039 K. Using eqs 1 and 4, the ordering temperature of $TbBi_{0.14}Ge_{1.74(2)}$ can be calculated as 15.4 K, close to the experimental result. The complex characters of the s−f exchange couplings and the slightly large deviation in Tb-germanides are probably due to the energy splitting and high energy level of Tb 4f bands, just 2 eV below the Fermi level.[50]

dx.doi.org/10.1021/ic400254v | Inorg. Chem. 2013, 52, 5307−5315

CONCLUSIONS

The new ternary phases $RE_2Al_{1-x}Ge_{2+x}$ (RE = Tb−Tm, Lu; $0.13(2) \leq x \leq 0.37(2)$) have been synthesized and structurally characterized. They crystallize with the W_2CoB_2-type structure in the space group *Immm*. This bonding arrangement is characterized by trigonal prisms of the rare-earth atoms centered by Ge atoms and distorted cubes of the rare-earth atoms centered by Al. The structure is not devoid of disorder, and Ge is shown to substitute 1/6 to 1/3 of the Al atoms. Similar 1:1 intergrowth of such fragments (AlB_2- and CsCl-types) is known for the RE_2XGe_2 (X = Mg, Cd, In) compounds with the Mo_2FeB_2-type structure. Electronic structure calculations corroborate the experimental findings. Correlations between the RE−RE separations and magnetic behaviors were established empirically based on the mean-field theory for antiferromagnets.

ASSOCIATED CONTENT

Supporting Information

Tables with atomic coordinates, equivalent displacement parameters, and occupancies for RE_2AlGe_2 (RE = Tb, Ho−Tm, Lu); tables with interatomic distances in RE_2AlGe_2 (RE = Tb, Ho−Tm, Lu); tables with principal thermal displacement parameters for RE_2AlGe_2 (RE = Tb, Er, Lu); figures showing experimental and simulated powder XRD patterns, elemental analyses, and magnetization vs temperature plots for samples with nominal compositions Dy_2AlGe_2 and $DyGe_3$. This material is available free of charge via the Internet at http://pubs.acs.org.

AUTHOR INFORMATION

Corresponding Author

*Fax: (302) 831-6335. E-mail: bobev@udel.edu.

Author Contributions

The manuscript was written through contributions of all authors. All authors have given approval to the final version of the manuscript.

Notes

The authors declare no competing financial interest.

ACKNOWLEDGMENTS

Svilen Bobev acknowledges financial support from the National Science Foundation through a grant DMR-0743916 (CAREER). We sincerely thank Mr. G. C. Shan (City University of Hong Kong) for his help with the structural optimizations.

REFERENCES

(1) (a) Guloy, A. M.; Corbett, J. D. *Inorg. Chem.* **1991**, *30*, 4789. (b) Salamakha, P. S.; Sologub, O. L.; Demcheko, P.; Righi, L.; Bocelli, G. *J. Alloys Compd.* **2001**, *315*, 1. (c) Budnyk, S.; Weitzer, F.; Kubata, C.; Prots', Yu.; Aksel'rud, L. G.; Schnelle, W.; Hiebl, K.; Nesper, R.; Wagner, F. R.; Grin', Yu. *J. Solid State Chem.* **2006**, *179*, 2329. (d) Mulder, F. M.; Thiel, R. C.; Buschow, K. H. J. *J. Alloys Compd.* **1994**, *205*, 169. (e) Tobash, P. H.; Meyers, J. J.; DiFilippo, G.; Bobev, S.; Ronning, F.; Thompson, J. D.; Sarrao, J. L. *Chem. Mater.* **2008**, *20*, 2151.

(2) (a) Tobash, P. H.; Lins, D.; Bobev, S.; Hur, N.; Thompson, J. D.; Sarrao, J. L. *Inorg. Chem.* **2005**, *45*, 7286. (b) Zhang, J.; Tobash, P. H.; Pryz, W.; Buttery, D.; Hur, N.; Thompson, J. D.; Sarrao, J. L.; Bobev, S. *Inorg. Chem.* **2013**, *52*, 953−964. (c) Christensen, J.; Lidin, S.; Malaman, B.; Venturini, G. *Acta Crystallogr., Sect. B: Struct. Sci.* **2008**, *64*, 272. (d) Shcherban, O.; Savysyuk, I.; Semuso, N.; Gladyshevskii, R.; Cenzual, K. *Chem. Met. Alloys* **2009**, *2*, 115. (e) Venturini, G.; Ijjaali, I.; Malaman, B. *J. Alloys Compd.* **1999**, *284*, 262. (f) Tobash, P. H.; Bobev, S.; Thompson, J. D.; Sarrao, J. L. *J. Alloys Compd.* **2009**, *488*, 533.

(3) Miller, G. J. *Eur. J. Inorg. Chem.* **1998**, 523.

(4) (a) Zaremba, V. I.; Kaczorowski, D.; Nychyporuk, G.; Rodewald, U. C.; Pöttgen, R. *Solid State Sci.* **2004**, *6*, 1301. (b) Tobash, P. H.; Lins, D.; Bobev, S. *Chem. Mater.* **2005**, *17*, 5567. (c) Suen, N. Z.; Tobash, P. H.; Bobev, S. *J. Solid State Chem.* **2011**, *184*, 2941. (d) Guo, S. P.; Meyers, J. J.; Tobash, P. T.; Bobev, S. B. *J. Solid State Chem.* **2012**, *192*, 16.

(5) Demchenko, G.; Konczyk, J.; Demchenko, P.; Kuprysyuk, V.; Gladyshevskii, R. *Acta Crystallogr., Sect. E: Struct. Rep. Online* **2006**, *62*, i55.

(6) Choe, W.; McWhorter, S.; Miller, G. J. *Z. Anorg. Allg. Chem.* **2002**, *628*, 1575.

(7) SMART, Bruker AXS Inc., Madison, WI, 2003.

(8) SAINT, Bruker AXS Inc., Madison, WI, 2003.

(9) SADABS, Bruker AXS Inc., Madison, WI, 2003.

(10) SHEXLTL, Bruker AXS Inc., Madison, WI, 2003.

(11) CIFs have also been deposited with Fachinformationszentrum Karlsruhe, 76344 Eggenstein-Leopoldshafen, Germany (fax: +49 7247 808 666; e-mail: crysdata@fiz.karlsruhe.de), depository numbers: CSD 425713 ($Tb_2Al_{0.87(2)}Ge_{2.13(2)}$); CSD 425714 ($Dy_2Al_{0.80(2)}Ge_{2.20(2)}$); CSD 425715 ($Ho_2Al_{0.77(2)}Ge_{2.23(2)}$); CSD 425716 ($Er_2Al_{0.67(2)}Ge_{2.33(2)}$); CSD 425717 ($Tm_2Al_{0.63(2)}Ge_{2.37(2)}$); CSD 425718 ($Lu_2Al_{0.79(1)}Ge_{2.21(1)}$).

(12) Tank, R.; Jepsen, O.; Burkhardt, A.; Andersen, O. K. The TB-LMTO-ASA program, version 4.7; Max-Plank-Institut fur Festkörperforschung, Stuttgart, Germany, 1994.

(13) Jepsen, O.; Andersen, O. K. *Z. Phys. B* **1995**, *97*, 35.

(14) Blöchl, P. E.; Jepsen, O.; Andersen, O. K. *Phys. Rev. B* **1994**, *49*, 16223.

(15) Dronskowski, R.; Blöchl, P. E. *J. Phys. Chem.* **1993**, *97*, 8617.

(16) Anderson, O. K.; Jepsen, O. *Phys. Rev. Lett.* **1984**, *53*, 2571.

(17) Lambrecht, W. R. L.; Andersen, O. K. *Phys. Rev. B* **1986**, *34*, 2439.

(18) Ordejón, P.; Artacho, E.; Soler, J. M. *Phys. Rev. B* **1996**, *53*, R10441.

(19) Soler, J. M.; Artacho, E.; Gale, J. D.; García, A.; Junquera, J.; Ordejón, P.; Sánchez-Portal, D. *J. Phys.: Condens. Matter* **2002**, *14*, 2745.

(20) Troullier, N.; Martins, J. L. *Phys. Rev. B* **1991**, *43*, 1993.

(21) Perdew, J. P.; Burke, K.; Emzerhof, M. *Phys. Rev. Lett.* **1996**, *77*, 3865.

(22) Kranenberg, C.; Mewis, A. *Z. Anorg. Allg. Chem.* **2000**, *626*, 1448.

(23) Reportedly, the RE_2AlSi_2 structures are ordered (ref 22), while we detected Al−Ge disorder in RE_2AlGe_2. Due to the very similar X-ray scattering factors of Al and Si, it is very likely that the Al site in the former is also occupied by the mixture of Al and Si atoms, instead of only Al atoms.

(24) Zhao, J. T.; Parthé, E. *Acta Crystallogr., Sect. C: Cryst. Struct. Commun.* **1990**, *46C*, 2276.

(25) Bauer, B.; Roehr, C. *Z. Naturforsch. B* **2011**, *66*, 793.

(26) Pauling, L. *The Nature of Chemical Bond*; Cornell University Press: Ithaca, NY, 1960.

(27) Mel'nyk, I.; Kuprysyuk, V.; Gladysheskii, R.; Pikus, S.; Staszuk, P. *J. Alloys Compd.* **2005**, *397*, 74.

(28) Zhao, J. T.; Parthé, E. *Acta Crystallogr., Sect. C: Cryst. Struct. Commun.* **1991**, *47*, 1781.

(29) Zhao, J. T.; Parthé, E. *Acta Crystallogr., Sect. C: Cryst. Struct. Commun.* **1991**, *47*, 1.

(30) Smart, J. S. *Effective Field Theories of Magnetism*; Saunders: Philadelphia, PA, 1966.

(31) $EuAl_4$ is an antiferromagnet with positive paramagnetic Curie temperature: Wernick, J. H.; Williams, H. J.; Cossard, A. C. *J. Phy. Chem. Solids* **1967**, *28*, 271.

(32) The magnetization of the Dy_2AlGe_2 sample shows another transition at uncharacteristically low temperature (ca. 15 K; see Figure

S3). It is very close to the ordering temperature of $DyGe_{1.5}$ (ca. 16 K),[1d] suggestive of the presence of a small amount impurity.
(33) de Gennes, P. G. *J. Phys. Radium* **1962**, *23*, 510.
(34) (a) Van Vleck, J. H. *The Theory of Electronic and Magnetic Susceptibilities*; Oxford University Press: London, 1965. (b) Gschneidner, K. A., Jr.; Eyring, L., Eds. *Handbook on the Physics and Chemistry of Rare Earths*; North Holland, Amsterdam, 1979; Vol. *2*.
(35) Buschow, K. H. J.; Schobinger-papamantellos, P.; Fischer, P. *J. Less-Common Met.* **1988**, *139*, 221.
(36) (a) Oleksyn, O.; Schobinger-Papamantellos, R.; Ritter, C.; de Groot, C. H.; Buschow, K. H. J. *J. Alloys Compd.* **1997**, *262*, 492. (b) Tobash, P. T.; DiFilippo, G.; Bobev, S.; Hur, N.; Thompson, J. D.; Sarrao, J. L. *Inorg. Chem.* **2007**, *46*, 8690.
(37) Schobinger-Papamantellos, P.; de Mooij, D. B.; Buschow, K. H. J. *J. Less-Common Met.* **1990**, *163*, 319.
(38) Oleksyn, O.; Schobinger-Papamantellos, R.; Ritter, C.; Janssen, Y.; Bruck, E.; Buschow, K. H. J. *J. Phys.: Condens. Matter* **1997**, *9*, 9993.
(39) Sekizawa, K. *J. Phys. Soc. Jpn.* **1966**, *21*, 1137.
(40) Zhang, J.; Hmiel, B.; Antonelli, A.; Tobash, P. H.; Bobev, S.; Saha, S.; Kirshenbaum, K.; Greene, R. L.; Paglione, J. *J. Solid State Chem.* **2012**, *196*, 586.
(41) Néel, L. *Nuovo Cimento, Suppl.* **1957**, *6*, 942.
(42) Wohlfarth, E. P., Eds. *Handbook of Magnetic Materials*; North Holland, Amsterdam, 1980; Vol. *1*.
(43) Lee, W. H.; Shelton, R. N.; Dhar, S. K.; Gschneidner, K. A., Jr. *Phys. Rev. B* **1987**, *35*, 8523.
(44) Mirambet, F.; Fournès, L.; Chevalier, B.; Gravereau, P.; Etourneau, J. *J. Magn. Magn. Mater.* **1994**, *138*, 244.
(45) Gallagher, K. A.; Willard, M. A.; Zabenkin, V. N.; Laughlin, D. E.; McHenry, M. E. *J. Appl. Phys.* **1999**, *85*, 5130.
(46) (a) Yosida, K.; Miwa, M. *J. Appl. Phys.* **1961**, *32*, 85. (b) Kaplan, T. A. *Phys. Rev.* **1961**, *124*, 329. (c) Elliott, R. J. *Phys. Rev.* **1961**, *124*, 346.
(47) We acknowledge the fact that the available distances used in the plot are from different temperatures. However, the variation from the temperature difference is very small.
(48) The overlap of distances within zone i is likely due to the structural parameters determined at different temperatures. Thus, the boundary is not exactly a point, but rather a range.
(49) Schobinger-Papamantellos, P.; de Mooij, D. B.; Buschow, K. H. J. *J. Alloys Compd.* **1992**, *183*, 181.
(50) Lang, J. K.; Baer, Y.; Cox, P. A. *J. Phys. F: Met. Phys.* **1981**, *11*, 121.